Journal of Magnetic Resonance 259 (2015) 163–173

Contents lists available at ScienceDirect

Journal of Magnetic Resonance

journal homepage: www.elsevier.com/locate/jmr

Gd(III) complexes for electron–electron dipolar spectroscopy: Effects of deuteration, pH and zero field splitting

Luca Garbuio [a], Kaspar Zimmermann [b], Daniel Häussinger [b], Maxim Yulikov [a,*]

[a] Laboratory of Physical Chemistry, ETH Zurich, Zurich, Switzerland
[b] Department of Chemistry, University of Basel, Basel, Switzerland

ARTICLE INFO

Article history:
Received 26 May 2015
Revised 6 August 2015
Available online 20 August 2015

Keywords:
Lanthanide
Gadolinium(III)
Pulse EPR
DEER
RIDME

ABSTRACT

Spectral parameters of Gd(III) complexes are intimately linked to the performance of the Gd(III)–nitroxide or Gd(III)–Gd(III) double electron–electron resonance (DEER or PELDOR) techniques, as well as to that of relaxation induced dipolar modulation enhancement (RIDME) spectroscopy with Gd(III) ions. These techniques are of interest for applications in structural biology, since they can selectively detect site-to-site distances in biomolecules or biomolecular complexes in the nanometer range. Here we report relaxation properties, echo detected EPR spectra, as well as the magnitude of the echo reduction effect in Gd(III)–nitroxide DEER for a series of Gadolinium(III) complexes with chelating agents derived from tetraazacyclododecane. We observed that solvent deuteration does not only lengthen the relaxation times of Gd(III) centers but also weakens the DEER echo reduction effect. Both of these phenomena lead to an improved signal-to-noise ratios or, alternatively, longer accessible distance range in pulse EPR measurements. The presented data enrich the knowledge on paramagnetic Gd(III) chelate complexes in frozen solutions, and can help optimize the experimental conditions for most types of the pulse measurements of the electron–electron dipolar interactions.

1. Introduction

A series of pulse techniques in electron paramagnetic resonance (EPR) that can be generally named as electron–electron pulse dipolar spectroscopy (PDS) [1–9] in combination with site directed spin labeling (SDSL) [10–13] is of great relevance in structural investigations of bio-macromolecules as such an approach furnishes distance information in the 1.5–12 nm range [14,15]. Stable nitroxide radicals are currently a common choice in SDSL-based studies, and the nitroxide–nitroxide double electron–electron resonance (DEER), a pulse EPR technique based on the use of two distinct excitation frequencies, is the most popular distance measurement technique [16,17]. Apart from DEER, the relaxation induced dipolar modulation enhancement (RIDME) [5–7] is a single-frequency technique that also detects static dipolar interaction, which can be then analyzed to get distances between spin labels. Other single-frequency experiments include the double quantum coherence (DQC) [8] and the SIFTER [9] techniques.

The PDS techniques can complement (and in some cases substitute) X-ray crystallography or NMR spectroscopy by providing long-range distance distributions in non-crystalline frozen solutions, in samples of low concentrations, down to a few μM, and with nearly any arbitrary molecular weight of the spin-labeled biomacromolecules [18–21]. In cases of the stand-alone application of PDS techniques coarse-grained structural models are obtained instead of the molecular structures at atomic resolution [22–24]. However, such PDS-based structural models can be capable of answering multiple biological questions. Elaborate signal assignment, as in NMR spectroscopy, is not necessary since the PDS signals originate uniquely from the spin labels.

A possible further advance in PDS methodology can be based on experiments with new spin labels with spectral characteristics different from the ones the nitroxide radicals. In the last decade it was shown that Gd(III) chelate complexes are suitable for nanometer-range distance measurements, especially at high fields and high frequencies [25]. In particular, an advantageous factor is the narrowing of the central resonance line in the Gd(III) EPR spectrum at increasing magnetic fields, which allows for better sensitivity and increased excitation bandwidth for a given power and duration of a microwave pulses. Contrary to nitroxide radicals, when using Gd(III) as spin labels, one can also benefit from the lack of orientation selection effects [26]. Importantly, the spectroscopic separation of Gd(III) centers from nitroxide radicals is possible, which allows for orthogonal distance measurement schemes [27–29]. Noteworthy, Gd(III) is relatively stable against reduction,

* Corresponding author.
E-mail address: maxim.yulikov@phys.chem.ethz.ch (M. Yulikov).

http://dx.doi.org/10.1016/j.jmr.2015.08.009
1090-7807/

making it favorable for in-cell studies, in which the cellular reducing environment is able to degrade nitroxide-based spin labels [30].

So far, most of the literature addressed the use of Gd(III) as contrast agents in magnetic resonance imaging (MRI) [31–40]. One important consequence of those activities was a development of bio-compatible Gd(III) tags. In the human body, the aqua ion $[Gd(H_2O)_9]^{3+}$ binds to endogenous chemical species leading to high in-vivo toxicity. For this reason, several cyclic chelating agents possessing high thermodynamic stability in complex with Gd(III) as well as kinetic inertness against ion dissociation have being developed [32].

Since Gd(III)-complexes have attracted growing attention for their use in PDS, a study of their spectroscopic properties regarding the dipolar spectroscopy applications is meaningful. The previous MRI-related studies concentrated on the number and properties of water protons in the first and second hydration sphere, which is not of direct interest for PDS. However, these MRI-related publications discussed to quite some extent the zero-field splitting (ZFS) in Gd(III) complexes, which is critically important for the PDS studies. In MRI, ZFS of Gd(III) centers was considered very important as it affects the Gd(III) electronic spin relaxation as well as the accuracy of the Gd(III)–water proton distance measurements [34]. Gd (III) echo-detected (ED) EPR spectra recorded at high fields were analyzed with respect of ZFS determination [35] and a stochastic superposition model was utilized to extract the characteristic ZFS parameters, D and E and their probability distributions, in glassy matrixes. In the spectra simulation, D was varied according to a Gaussian distribution (or a bimodal distribution consisting of two Gaussians with positive and negative mean D value) and the E/D distribution could be approximated by a second order polynomial [35]. EPR experiments at 240 GHz allowed Benmelouka et al. [36] to determine the magnitude and sign of the ZFS parameters in frozen solutions for several Gd(III)-complexes. A correlation between complex symmetry and sign of D was established [36].

In solution, it was proposed that a time-dependent or transient ZFS [37] acts in addition to a time-independent or static ZFS [38]. Whereas the former arises from the perturbation of the ligands field due to instantaneous distortions or vibrations, the latter, due to the static crystal field, is modulated by the Brownian motion and rotation of the complex and it was found dependent on the nature of the ligands [39]. The study of the ZFS interaction in these complexes is complicated by the contemporaneous presence of structural isomers and different sets of ligand-field parameters. Multiple-frequency continuous-wave (CW) EPR investigations were performed in order to evaluate the contribution of the static and transient ZFS in the temperature range 276–350 K [39]. It was suggested that inter-conversion between coordination geometries does not affect the magnitude of the transient ZFS which should be dominated by faster processes such as vibrations and as a consequence, coordination isomers are indistinguishable at any EPR field strength [40].

Here we are interested in discussing the effect of ZFS term on the performance of PDS experiments. As just mentioned, ZFS affects heavily the appearance of the Gd(III) ED EPR spectrum. The spectrum is characterized by a narrow peak, arising from the central transition $|-1/2\rangle \leftrightarrow |+1/2\rangle$, and by a broad background connected to the other six remaining transitions [34,41]. The magnitude of the ZFS influences the width of the central transition, which in turn affects sensitivity and modulation depth in DEER experiments since the excitation bandwidth of the microwave pulses is limited. In PDS measurements the detection frequency (or the pump frequency in DEER) is typically set at the maximum absorption of Gd(III) ED EPR spectrum where the central transition $|-1/2\rangle \leftrightarrow |+1/2\rangle$ dominates. A weak ZFS is thus desirable to allow for a higher fraction of spins to be pumped or observed.

Experimental observations seem to suggest an effect of the ZFS magnitude on the DEER echo reduction effect in Gd(III)–nitroxide DEER experiments [28,42]. This phenomenon, i.e. the intensity reduction of the refocused echo upon application of the pump pulse, is one of the main factors that affects the sensitivity of the Gd(III)–nitroxide DEER method at X and Q band. The detection in this case is performed on the Gd(III) centers and the pump pulse acts on the nitroxide species. In nitroxide–nitroxide DEER experiments the DEER echo reduction is described by the Bloch–Siegert effect [43,44]. The off-resonant pump pulse produces dynamic phase shifts of spin packets that are forming the refocused echo, thus resulting in a partial echo defocusing. Since in Gd(III)–nitroxide DEER low-spin ($S = 1/2$) nitroxide radicals require significantly higher microwave power than Gd(III) centers, the known Bloch–Siegert effect is stronger in this case compared to the nitroxide–nitroxide or Gd(III)–Gd(III) DEER experiments [45]. However, at least at Q band, the DEER echo reduction in Gd(III)–nitroxide case depends on the strength of ZFS interaction of Gd(III) centers and thus cannot be exclusively caused by the Bloch–Siegert effect [43,44].

The PDS experiments with Gd(III) centers are performed at cryogenic temperatures. Thus, relaxation properties of Gd(III) approximately in the range 5–30 K are of particular importance for these EPR techniques. Raitsimring et al. [46] recently proposed that the mechanism concurring to the Gd(III) phase memory time is transition dependent. At W band the contribution to the relaxation of the $|-1/2\rangle \leftrightarrow |+1/2\rangle$ transition was suggested to be dominated by nuclear spin diffusion, whereas other transitions were analyzed according to a ZFS-driven relaxation mechanism. The ZFS-driven relaxation at the central transition might contribute more strongly at Q band (35 GHz) than at W band (95 GHz) as this contribution would scale down with the ZFS-induced anisotropy of the central transition, which decreases proportional to $D^2/((g\beta)^2B_0)$. Since the central transition is influential in PDS with Gd (III), the determination of the interplay between different relaxation mechanisms is of interest. In particular, the nuclear spin diffusion drives electron transverse relaxation trough stochastic fluctuations of hyperfine fields, thus, the level of deuteration of the sample can influence the relaxation properties of Gd(III). As deuterons possess a smaller magnetic dipole moment than protons, deuteration slows down the phase memory time of the observed species and it is thus used to increase the longest measurable length of the DEER trace [15,47]. This way one can extend the upper distance limit reachable by PDS and improve sensitivity. The longitudinal relaxation time of Gd(III) centers (T_1) is also important since it is directly connected to the minimal possible shot repetition time (i.e. the time in DEER between an experiment and the next for a given pump position). A shorter T_1 allows thus to decrease the experimental time needed to obtain a certain signal-to-noise ratio (S/N).

The purpose of this paper is to inspect the spectroscopic properties of Gd(III) chelate complexes at conditions that are relevant for PDS experiments. We particularly focus on DOTA (1,4,7,10-tetra azacyclododecane-1,4,7,10-tetraacetic acid) because it is the most common cyclic complexing agent for Gd(III) and $[Gd(DOTA)]^-$ is frequently employed in DEER measurements [48]. Upon chemical modification of the basic structure of DOTA, several derivatives can be obtained. Representatives of this family are DOTAM (1,4,7, 10-tetrakis(carbamoylmethyl)-1,4,7,10-tetraazacyclododecane), M8DOTA [49] and DOTP (1,4,7,10-tetraazacyclododecane-1,4,7,10-tetra(methylene phosphonic acid)) (Fig. 1) that we tested to obtain a systematic comparison with DOTA. We report a series of measurements at Q band, which is one of the regularly used microwave bands for measurements with Gd(III) and we concentrate on the temperature of 10 K, used in several previous studies [29,50,51]. First, the determination of the ZFS parameters is performed for

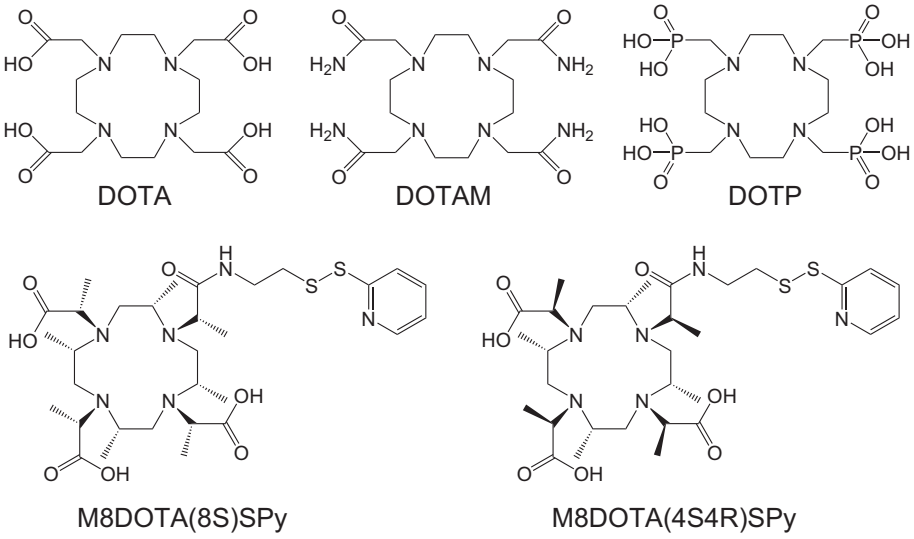

Fig. 1. Chemical structures of the investigated chelating agents.

the above listed Gd(III)-complexes. Second, an experimental picture of the impact of matrix deuteration on relaxation times T_2, T_1 at the maximum intensity point of the Gd(III) spectrum is given. Next, the values of the Gd(III)–nitroxide DEER echo reduction are reported and a correlation with the ZFS magnitude is proposed. After this we provide reference data on the dependence of the relaxation parameters (T_1, T_2) on pH in a biologically-pertinent range. And finally we compare longitudinal and transverse relaxation of different complexes in a D_2O/glycerol-d_8 glassy matrix at 10 K.

2. Materials and methods

2.1. Chemicals

The following acronyms will be used: DOTA, 1,4,7,10-tetraazacyclododecane-1,4,7,10-tetraacetic acid; DOTP, 1,4,7,10-tetraazacyclododecane-1,4,7,10-tetra(methylene phosphonic acid); DOTAM, 1,4,7,10-tetrakis(carbamoylmethyl)-1,4,7,10-tetraazacyclododecane; MES, 2-(*N*-morpholino)ethanesulfonic acid; Xylenol Orange, 3,3′-Bis[N,N-bis(carboxymethyl)aminomethyl]-o-cresolsulfonphthalein disodium salt. M8DOTA(8S)SPy, (2*S*,2′*S*,2″*S*)-2,2′,2″-((2*S*,5*S*,8*S*,11*S*)-2,5,8,11-tetramethyl-10-((*S*)-1-oxo-1-((2-(pyridin-2yldi-sul-fanyl)-ethyl)amino) propan-2-yl)-1,4,7,10-tetraazacyclo-dodecane-1,4,7-triyl)tripropanoic acid; M8DOTA(4R4S)SPy, (2*R*,2′*R*,2″*R*)-2,2′,2″-((2*S*,5*S*,8*S*,11*S*)-2,5,8,11-tetramethyl-10-((*R*)-1-oxo-1-((2-(pyridin-2yldi-sul-fanyl)-ethyl)amino) propan-2-yl)-1,4,7,10-tetraazacyclo-dodecane-1,4,7-triyl)tripropanoic acid; when simultaneously referring to both M8DOTA(8S)SPy and M8DOTA(4R4S)Spy ligands, an abbreviation M8DOTA will be used. Unless stated otherwise, all commercially available chemicals were used as received. M8DOTA ligands were synthesized according to Ref. [49]. DOTA·$6H_2O$, DOTP and DOTAM were purchased from Macrocyclics, Dallas. $GdCl_3·6H_2O$ (99.99%), MES (99.5%), sodium acetate (>99%), D_2O (99.9%, d_2) were purchased from Sigma–Aldrich. Glycerol ($C_3H_8O_3$, 99%) was purchased from Honeywell. Perdeuterated glycerol-d_8 ($C_3D_8O_3$, 98%) was purchased from Isotec. Xylenol Orange was purchased from TCI. The buffer was prepared as follow: 1 g of MES was dissolved in 20 ml of H_2O or D_2O. The pH of the corresponding solution (250 mM) was adjusted to 5.8 with 0.1 M NaOH aqueous solution (H_2O or D_2O). At this pH, precipitation of Gd(III)–hydroxides during sample preparation is prevented. MES was used as it does not coordinate to Gd(III).

2.2. Gd(III)-complex formation

The molecular structures of the studied ligands and corresponding abbreviated names are shown in Fig. 1. [Gd(M8DOTA(8S)SPy)] and [Gd(M8DOTA(4R4S)SPy)] were prepared in aqueous buffered solution (100 mM ammonium acetate) according to Ref. [49]. Due to the extremely high affinity of the M8DOTA-ligands to gadolinium ions, the resulting [Gd(M8DOTA)] complexes could be purified by HPLC followed by a Sep-pak-C18 column (Waters) for desalting. Aqueous solutions of the [Gd(M8DOTA)] complexes were mixed with the corresponding buffer, the pH was adjusted, the solution was lyophilized and the final concentration was obtained by dissolving in the desired amount of water (H_2O or D_2O) and glycerol-d_8 All other gadolinium complexes were prepared as follows. 300 µl of a 128 mM buffer solution of $GdCl_3·6H_2O$ (38.4 µmol, 1 eq.) were added to 1 ml of a 50 mM buffer solution of chelating agent (50 µmol, 1.3 eq.). The solution was stirred for 24 h. The presence of non-chelated Gd(III) ions was detected from the color of the solution by eye using xylenol orange as indicator according to the procedure described earlier [52]. 100 µl of the Gd(III)-complex solution were diluted with 1.2 ml of a 50 mM acetate buffer solution at pH = 5.8 and few drops of a 0.016 mM xylenol orange solution were added. An orange color of the resulting solution was indicative of the negligible presence of Gd(III) aquo-ions. Next, 10 µl of the Gd(III)-complex solution were diluted to 490 µl of buffer solution. To 25 µl of this solution were added 25 µl of glycerol (or glycerol-d_8) in order to obtain a final concentration of ~300 µM Gd(III)-complex in 1/1 volume-to-volume buffer/glycerol mixture. The addition of glycerol is necessary for EPR samples to form a glassy matrix and thus a homogeneous distribution of Gd(III) species upon shock freezing. EPR quartz tubes of outer diameter of 2.95 mm were filled with the desired sample and finally shock frozen by immersion into liquid nitrogen. Samples were stored at −80° C. In the course of this paper, the binary solvent system buffer/glycerol will be simply referred to as glassy matrix and the contained isotopologues (H_2O *vs.* D_2O and glycerol *vs.* glycerol-d_8) will be specified on a case-by-case basis.

2.3. Relaxation time traces

All EPR measurements reported here were performed at 10 K with a home-built high-power Q-band spectrometer [53] equipped with a rectangular cavity that allows for oversized samples [54].

Table 1
Magnitudes of $\langle D\rangle$ and σ parameters used in simulations of the ED EPR spectra for different Gd(III) complexes. The spectra of Gd(III) centers were simulated by assuming a bi-Gaussian distribution of the D parameter centered at the mean values $\pm\langle D\rangle$ with the standard deviation σ and a second order polynomial for the E/D distribution (see text). As an exception, the ED EPR spectrum for DOTP was simulated by assuming two Gaussian distributions with different $|\langle D\rangle|$ and σ.

Chelating agent	$\langle D\rangle$ (MHz)	σ
DOTAM	560	$\langle D\rangle/3.5$
DOTA	685	$\langle D\rangle/3$
M8DOTA(4R4S)SPy	890	$\langle D\rangle/4$
M8DOTA(8S)SPy	1260	$\langle D\rangle/4$
DOTP	$D_1 = -750$ (60%)	$D_1/3$
	$D_2 = +1950$ (40%)	$D_2/10$

The sample temperature was stabilized with a He-flow cryostat (ER 4118CF, Oxford Instruments). The T_2 time traces were obtained by a Hahn echo sequence with the pulse durations $(\pi/2) = 16$ ns and $(\pi) = 32$ ns. T_1 time traces were recorded with an inversion recovery experiment with an inversion π-pulse of 32 ns and detection sequence of $(\pi/2) = 52$ ns and $(\pi) = 104$ ns. Relaxation time traces were recorded at the intensity maximum of Gd(III) ED EPR spectrum.

2.4. Echo detected EPR spectra

ED EPR spectra of Gd(III) complexes were recorded with the Hahn echo detection sequence at different pulse lengths and at different interpulse delays d_1 (i.e. the time between the first and the second pulse in the Hahn echo sequence). We used 'hard' ($\pi/2 = 12$ ns, $\pi = 12$ ns) and 'soft' ($\pi/2 = 16$ ns, $\pi = 32$ ns) pulses to check for any differences due to the change of the excitation bandwidth. Simulations of the ED EPR spectra were carried out according to the previously described procedure [28] with a home-written program based on EasySpin function 'pepper' [55]. Spectra were computed by using a bimodal distribution consisting of two Gaussian distributions of the D parameter centered at the mean value $\langle D\rangle$ and $-\langle D\rangle$, with the same standard deviation σ in both cases (with an exception for DOTP that is explained in the Results section). A second order polynomial form of the E/D distribution: $P(E/D) \propto (E/D) - 2(E/D)^2$ was used [28,55]. The simulation parameters are listed in Table 1.

2.5. Echo reduction effect

Echo reduction experiments (Fig. 2) were performed by running a static four-pulse DEER scheme [3,4] with $\pi/2 = 12$ ns, $\pi = 12$ ns pulses and a $+x/-x$ phase cycle on the first pulse. The time position of the pump pulse was set to overlap with the primary echo and was kept fixed during the echo intensity measurement (i.e. the first inter-pulse delay was set to 400 ns, and the pump pulse position was at 800 ns after the $\pi/2$ pulse). It has been checked experimentally that the reduction of the Gd(III) DEER echo is not dependent on the presence of nitroxide species [28], therefore the experiment was set up for the samples with only Gd(III) chelate complexes present. At the pump frequency, to set the proper microwave power for the inversion pulse, a 12 ns π pulse was set at the maximum intensity of the Gd(III) spectrum, then the microwave power was increased by 12 dB by opening a precise attenuator (this was the experimentally estimated difference in the power between Gd(III) and nitroxide species), and the detection field was reduced by 11 mT in order to put the spectral position of the pump pulse at the place that would correspond to the maximum of the nitroxide spectrum at given settings. Detection frequency was set 300 MHz lower than the pumping frequency, which corresponded to the maximum intensity of the Gd(III) spectrum. Such pulse settings were typically employed in previously reported Q-band Gd(III)–nitroxide DEER experiments in our group [27]. At this

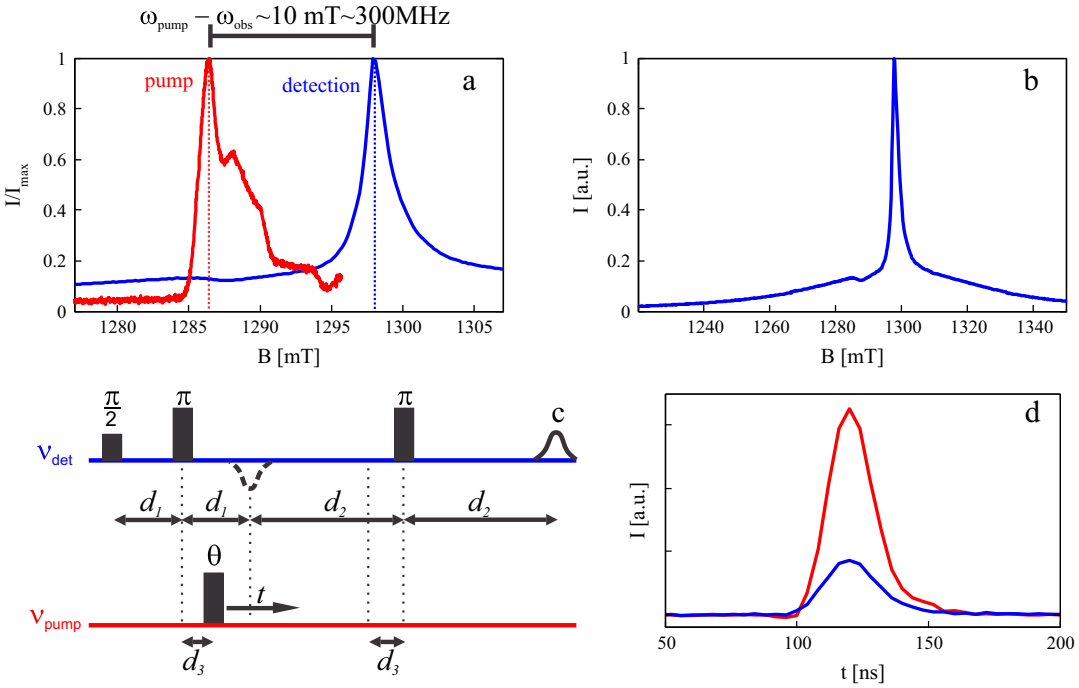

Fig. 2. (a) ED EPR spectrum of $[Gd(DOTA)]^-$ (blue) and nitroxide (red) at 10 K at Q band. The frequency offset between pump and detection frequency is approximately 300 MHz. (b) ED EPR spectrum of $[Gd(DOTA)]^-$ in a larger magnetic field range. (c) Pulse sequence in the Gd(III)–nitroxide DEER experiment. The detection pulses (blue) are set on intensity maximum of Gd(III) ED EPR spectrum and the pump frequency (red) at the maximum of nitroxide ED EPR spectrum. θ is the nominal flip angle of the pump pulse. (d) Echo reduction effect in [Gd(M8DOTA(8S)SPy)]: the shape of the refocused echo in the DEER experiment with (blue) and without (red) the pump pulse $\theta = \pi$ applied. (For interpretation of the references to color in this figure legend, the reader is referred to the web version of this article.)

frequency offset, for the resonator used, 12 ns was the shortest systematically achievable duration of detection pulses. In the following, the echo reduction is expressed in percent ratio between the intensity of the echo with and without applying the inversion pulse on the pump frequency.

3. Results

3.1. Determination of the ZFS magnitude of Gd(III)-complexes

First, we determined the strength of the ZFS interaction in the discussed series of macrocyclic complexes (Fig. 1). The experimental ED EPR spectra of $[Gd(DOTAM)]^{3+}$, $[Gd(DOTA)]^{-}$, two stereoisomers of [Gd(M8DOTA)] and $[Gd(DOTP)]^{5-}$ and corresponding simulations are shown in Fig. S1. The parameters used in these simulations are listed in Table 1. The $\langle D\rangle$ value for DOTA is consistent with our previous calculations [42] and with the prior results of other authors [35,36], thus confirming the validity of the ZFS determination approach. The strength of obtained characteristic $|\langle D\rangle|$ values for these macrocyclic complexes follows the trend DOTAM < DOTA < M8DOTA(4R4S)SPy < M8DOTA(8S)SPy < DOTP (Table 1). Note however, that for DOTP a different type of the bimodal distribution had to be used in simulation with one Gaussian component characterized by $|\langle D_1\rangle|$ = 750 MHz and $\sigma_1 = D_1/3$, and the other component characterized by $\langle D_2\rangle$ = +1950 MHz and $\sigma_2 = D_2/10$. The relative weight of the first component of 60% and second component of 40% was used in the simulation shown in Fig. S1. Despite the two-component simulation, the discrepancy between the simulation and the experimental ED EPR spectrum is still somewhat worse for $[Gd(DOTP)]^{5-}$ sample, as compared to other four (Fig. S1). Importantly, only the second component has a $\langle D\rangle$ value that is larger in absolute magnitude than the one for M8DOTA(8S). The sign of the second component determines the type of the asymmetry of the ED EPR spectrum of $[Gd(DOTP)]^{5-}$ complex and could be assigned to be positive. The sign of the $\langle D_1\rangle$ value is less critical to the overall shape of the spectrum and thus it could not be determined with certainty. The simulation presented in Fig. S1 was performed with a negative $\langle D_1\rangle$ value. For the symmetric bimodal distributions of D values (DOTA, DOTAM, M8DOTA) the estimated error is between 5% and 10% for $\langle D\rangle$ and between 10% and 20% for σ. For DOTP we estimate a larger error between 10% and 20% for $\langle D_1\rangle$ and $\langle D_2\rangle$ and an error between 30% and 40% for σ_1 and σ_2 values.

3.2. Effect of matrix deuteration on the relaxation of $[Gd(DOTA)]^{-}$

In order to better understand the effect of deuteration on relaxation properties of Gd(III) centers, we performed a series of experiments with $[Gd(DOTA)]^{-}$. Fig. 3 shows the transverse and longitudinal relaxation time traces in linear and semi-logarithmic representation obtained for $[Gd(DOTA)]^{-}$ in glassy matrix water/glycerol (1:1 v/v). The longitudinal relaxation is very weakly changing upon deuteration of the solvent. The same outcome was reported on nitroxide-labeled LHCIIb [56] where T_1 of the nitroxide radicals were virtually unaffected by buffer deuteration. In the latter case the small or even insignificant change in longitudinal relaxation was rationalized by evaluating that T_1 is mainly driven by fluctuations of the hyperfine field induced by libration motion of nitroxide moiety [57]. Here, similarly, the thermal fluctuations of orbit-lattice coupling in Gd(III) centers should be responsible for the main contribution to the longitudinal relaxation at cryogenic temperatures, so that the hyperfine interactions with the magnetic nuclei of solvent molecules exert only a very small impact on T_1.

In contrast to longitudinal relaxation, the transverse relaxation traces manifest a remarkable sensitivity to proton/deuterium relative concentration (Fig. 3), again comparable to the effect observed on nitroxide spin labels [15,47]. This has an important consequence for the DEER technique because a longer T_2 of the detected species (Gd(III) ions in the Gd(III)–nitroxide DEER) allows detection of longer distances and better sensitivity. In the case at hand, a length of the DEER trace of 12–13 μs should be possible, thus

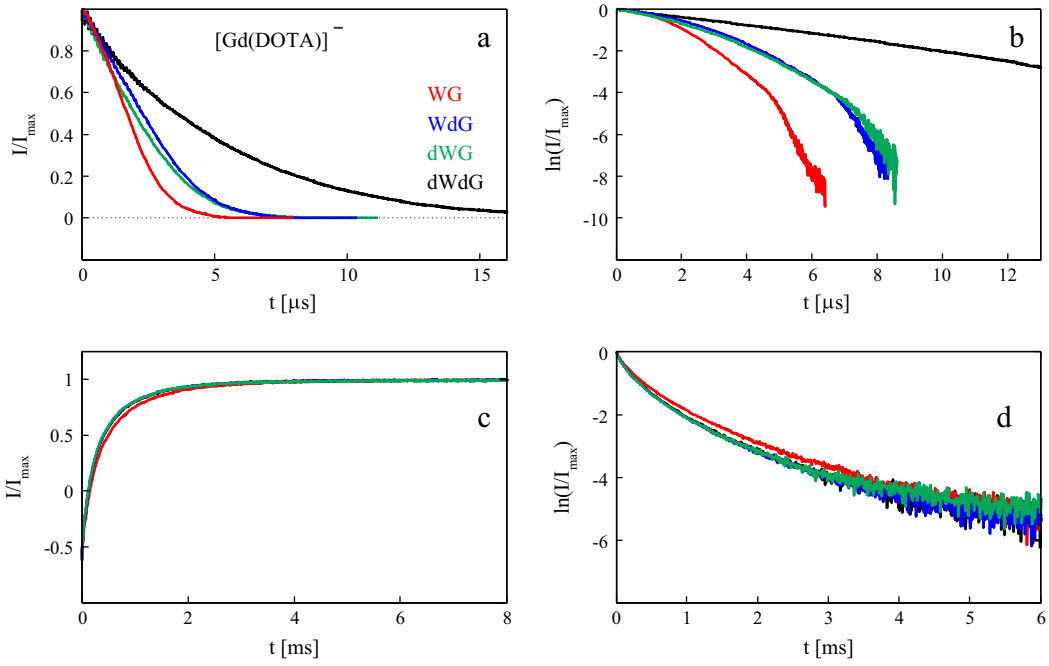

Fig. 3. Solvent dependency of the transverse (a and b) and longitudinal (c and d) relaxation time traces of $[Gd(DOTA)]^{-}$ in linear (a and c) and semilogarithmic (b and d) representation. Measurements were recorded at 10 K at Q band at pH 5.8 and in different solvents: red (H_2O/glycerol), blue (H_2O/glycerol-d_8), green (D_2O/glycerol) and black (D_2O/glycerol-d_8). Each time trace was normalized to its maximum. The codes in the figure legend stand for 'd' deuterated, 'W' water, and 'G' glycerol. (For interpretation of the references to color in this figure legend, the reader is referred to the web version of this article.)

allowing for detection of distances up to ~8 nm. If only one of the two solvents in the mixture is deuterated, the combination H_2O/glycerol-d_8 reveals a slightly more beneficial transverse relaxation than the combination D_2O/glycerol in the intermediate delay times range (Fig. 3). This might be an indication of some differences in solvation of the Gd(III) complexes by glycerol and by water molecules. Fig. 3 shows that in both H_2O/glycerol-d_8 and D_2O/glycerol matrices at the times longer than 4 μs, the longest feasible transverse evolution times, the two time traces are very similar. In these two cases the longest detectable distance and the signal-to-noise ratio in a DEER experiment with Gd(III) centers would be thus nearly the same.

The transverse relaxation time trace recorded in a fully protonated matrix presents a characteristic curvature at the initial range of times, more visible in the semi-logarithmic plot, suggesting a significant impact of the nuclear spin diffusion mechanism to transverse relaxation. When the D_2O/glycerol-d_8 matrix is used, the trace assumes a "mono-exponential" character, almost linear in the semi-logarithmic plot (Fig. 3).

It was suggested that at W band the relaxation of the central transition of $[Gd(DOTA)]^-$ is dominated by the nuclear spin diffusion mechanism [46]. At Q band we clearly observe a change of the dominating relaxation mechanism. In the fully protonated matrix, transverse relaxation is dominated by the nuclear spin diffusion, whereas it seems to be dominated by the ZFS-driven, or, perhaps, ligand hyperfine-driven mechanism in the fully deuterated matrix. Importantly, at W band the transverse relaxation at the central transition was also almost mono-exponential (linear in the semi-logarithmic plot) [46]. Note also a slower relaxation reported at W band [46] as compared to our Q-band data. This might be related to the reduction of ZFS-driven relaxation contribution for the central transition of Gd(III) at increased detection frequency. These observations suggest that the assumption of the dominating impact of nuclear spin diffusion on the transverse relaxation of the central transition of $[Gd(DOTA)]^-$ in deuterated matrix [46] might be an overestimation. For Gd(III) complexes with ZFS stronger than that of $[Gd(DOTA)]^-$ the transverse relaxation of the central transition in fully deuterated matrix might still be ZFS-driven at W band.

As discussed by Raitsimring et al., the ZFS-driven contribution to the relaxation of the central transition of Gd(III) should always be weaker than for the other transitions [46]. Nonetheless, if the main mechanism of the transverse relaxation of the central transition is not the same as for the other transitions, both faster and slower rates might be possible. An example of such a case is demonstrated in Fig. 4. The value R is calculated as a ratio between the Hahn echo intensity at the maximum of Gd(III) spectrum and at the position of the 'kink' (indicated by an arrow and an asterisk), where the contribution of the central $|-1/2\rangle \leftrightarrow |+1/2\rangle$ transition of Gd(III) is close to zero, but all other transitions do contribute to the intensity of the electron spin echo. Note that here we don't make a detailed decomposition into the individual transitions, since the qualitative picture to be drawn is clear enough without such a data processing: first, the central transition initially contributes at least 80% of the echo intensity at the maximum of the $[Gd(DOTA)]^-$ spectrum; second, transverse relaxation of all the other transitions is ZFS-driven (at least in a deuterated matrix [46]) so that for qualitative conclusions they can be considered together, indicating thus an average ZFS-driven relaxation rate. Fig. 4a demonstrates that in a fully protonated solvent mixture the value R is continuously decreasing with the increase of the interpulse delay time τ, and, from the shape of the ED EPR spectrum at $\tau = 5$ μs, one can conclude that the coherence formed on the central transition of Gd(III) has completely decayed while the other transitions still provide a detectable echo signal. This implies that in a protonated matrix the transverse relaxation of the central

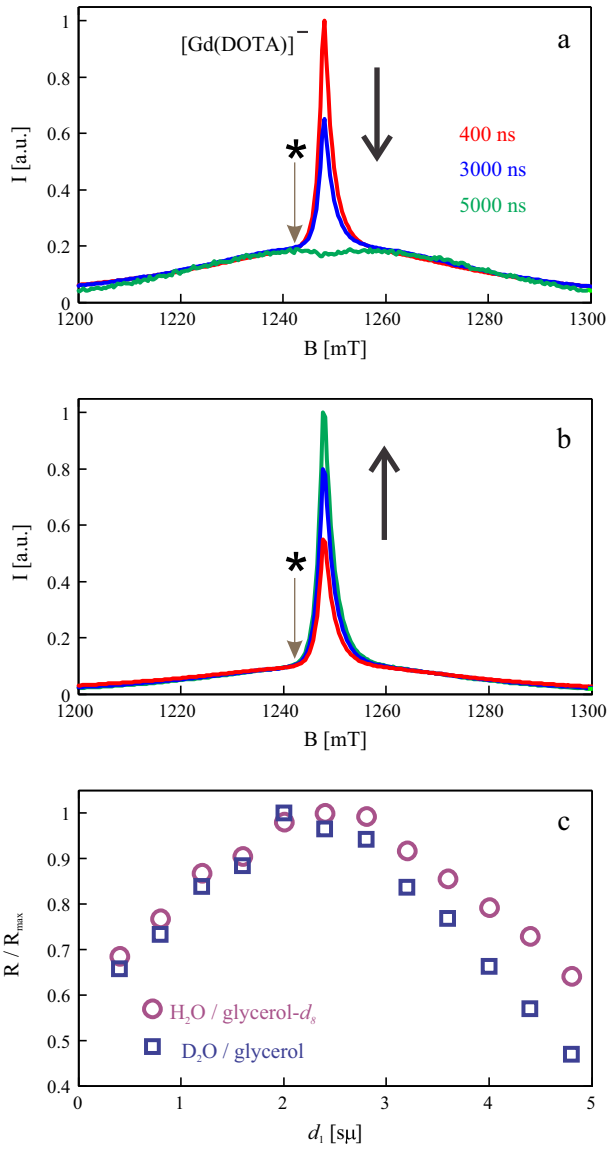

Fig. 4. Dependency of the ED Q-band EPR spectra of $[Gd(DOTA)]^-$ on the solvent deuteration. Spectra were recorded at 10 K in a Hahn echo experiment with different interpulse delays d_1 and with lengths of both m.w. pulses of 12 ns. (a) H_2O/glycerol; (b) D_2O/glycerol-d_8; red: $d_1 = 400$ ns, blue: $d_1 = 3000$ ns, green: $d_1 = 5000$ ns. Spectra were normalized in order to reach the same intensity for each spectrum of the outer transitions of Gd(III) at the point marked with the brown arrow and asterisk (see text for details). (c) Dependency of the relative intensity of the central transition of $[Gd(DOTA)]^-$ on the Hahn echo delay time. Spectra were recorded at 10 K with different interpulse delays and both pulse lengths of 12 ns. Purple circles: H_2O/glycerol-d_8; dark blue squares: D_2O/glycerol. The value R stays for the ratio between the intensity at the maximum of the Gd(III) ED EPR spectrum and the intensity close to the 'kink' of the central transition, as indicated by brown arrow and asterisk in (a and b). (For interpretation of the references to color in this figure legend, the reader is referred to the web version of this article.)

transition is dominated by the spectral diffusion, and that this contribution is stronger for the central transition than for the other ones. Moreover, the spectral diffusion-driven relaxation of the central transition is faster than the ZFS-driven relaxation of other transitions. For the fully deuterated solvent mixture (Fig. 4b) the picture is opposite and the contribution of the central transition of the Gd(III) grows with the increase of τ. Qualitatively analogous behavior was observed for DOTAM, M8DOTA and DOTP complexes.

A transition between the two regimes can be observed in the glassy matrix having only one component (water or glycerol) deuterated (Fig. 4c). In both D_2O/glycerol and H_2O/glycerol-d_8

matrices, experiments reveal that the transverse relaxation of the central transition is slower than for the other transitions only for short interpulse delays. For delay times longer than ~2.5 μs, the central transition of Gd(III) begins to decay faster than other transitions. This second decay regime is more pronounced in the D_2O/glycerol matrix (compared to H_2O/glycerol-d_8) thus suggesting heterogeneous complex solvation, with glycerol residing on average closer to the macrocycle than water. These different relaxation regimes of the Gd(III) central transition need to be taken into account whenever a detailed analysis of the Gd(III) spin dynamics is to be performed. In particular, DEER experiments with shaped broad band microwave pulses were recently proposed that might require correction for such transition-dependent relaxation in their setup and analysis [58–61]. Note also that the ED EPR spectra in the investigated four different matrices overlap perfectly at short interpulse delays of d_1 = 400 ns regardless of the pulse length (see SI, Fig. S2).

3.3. DEER echo reduction

The Bloch–Siegert mechanism of the reduction of refocused echo upon the application of pump pulse describes the frequency-dependent phase shift for detected spins due to the interference with the pump pulse [43,44]. This effect appears in cases of partial overlap of the excitation profiles of the pump and detection pulses in the DEER experiment. In addition to the Bloch–Siegert mechanism, relevant for any spin, the second proposed echo reduction mechanism [28] is related to the spin dynamics of e.g. the high-spin Gd(III) system. It was suggested that upon application of the pump pulse, single-quantum coherences of Gd(III) could be transferred to non-detectable double-quantum and higher coherences, which leads to an additional reduction of the echo amplitude. Simulations of the echo reduction effect [28,42] that took into account the Bloch–Siegert shift and the magnetization loss to multiple-quantum coherences of the Gd(III) high-spin, were able to partially reproduce the intensity drop of the echo in $[Gd(DTPA)]^{2-}$ complexes (DTPA = diethylene triamine pentaacetic acid) additionally suggesting that other interactions should be considered for a full understanding of the phenomenon. It is thus of interest to study the impact of deuteration on the echo reduction in Gd(III) centers. Here we report echo reduction data for different interpulse delays at 10 K at Q band. Measurements carried out on $[Gd(DOTA)]^-$ (first four lines in Table 2) indicate not only that deuteration plays a role but also that this effect is virtually independent on the mixing time. Note that the values reported in Table 2 must be taken only as indicative numbers. The outcome of the DEER echo reduction measurement is sensitive to the shape of the low-frequency wing of the microwave resonator dip. Absolute values of echo intensity vary thus between different measurement sessions. In addition, values obtained for long mixing times suffer from bigger uncertainties due to the difficulty in tuning the echo phase for lower signals. In spite of this variability, the overall trend of the DEER echo reduction effect is always maintained so that, for example, DOTA shows always a weaker reduction effect in fully deuterated matrices in comparison with protonated matrices. These observations ultimately suggest that hyperfine interactions of nuclei surrounding the complex do play a role in the echo reduction effect.

A series of echo reduction measurements on DOTAM, M8DOTA and DOTP also indicates a dependency of this effect on the magnitude of ZFS in a fully deuterated matrix. Namely, the comparison of values in Tables 1 and 2 shows that the echo reduction is generally weaker for Gd(III)-complexes with stronger ZFS. Following the rule, DOTAM that has the weakest ZFS in the series at the same time has the strongest echo reduction: only about 5% of the DEER echo intensity is left if the pump pulse is applied. For Gd(III)–nitroxide distance measurements with such complexes the use of modified DEER sequence with reduced flip angle of the pump pulse would be recommended [29].

Table 2
Echo reduction effect for the investigated samples at different interpulse delays d_2. Echo reduction is expressed in % ratio between the intensity of the echo with and without applied pump pulse.

Matrix	Chelating agent	Interpulse delay time		
		1.2 μs	3 μs	4 μs
H_2O/glycerol	DOTA	9	6	9
H_2O/glycerol-d_8	DOTA	12	11	11
D_2O/glycerol	DOTA	13	14	11
D_2O/glycerol-d_8	DOTA	17	18	18
D_2O/glycerol-d_8	M8DOTA(8S)SPy	19	20	n.d.
D_2O/glycerol-d_8	M8DOTA(4S4R)SPy	15	14	n.d.
D_2O/glycerol-d_8	DOTAM	5	6	5
D_2O/glycerol-d_8	DOTP	35	28	28
D_2O/glycerol-d_8	H_2O	24	24	n.d.

3.4. Effect of pH on relaxation times and ED EPR spectra of $[Gd(DOTA)]^-$

Since interaction with surrounding protons is the dominating mechanism of transverse relaxation of the central transition of Gd(III) in a fully protonated matrix, we tested the effect of pH on the relaxation and ED EPR spectrum of $[Gd(DOTA)]^-$, based on the assumption that solvation of Gd(III) complexes should depend on pH. Fig. 5 shows the transverse and longitudinal relaxation time traces of $[Gd(DOTA)]^-$ in linear and semi-logarithmic plots. One can observe in Fig. 5 that while no significant change in longitudinal relaxation takes place upon using different pH, from 5.8 to 9, the shape of the transverse relaxation time trace reveals small but measurable pH dependency.

At acidic pH (pH = 5.8), the transverse relaxation shows largest non-linearity in the semi-logarithmic plot and can thus be considered to contain strongest contribution from spectral diffusion. At neutral (pH = 7) and basic (pH = 9) conditions the transverse relaxation traces are more linear in the semi-logarithmic coordinates, however not yet very close to a mono-exponential (linear) behavior.

The ED EPR spectrum of $[Gd(DOTA)]^-$ did not reveal any pH dependence. Concerning the relatively slow kinetics of the $[Gd(DOTA)]^-$ complex formation [62,63] no changes in the ED EPR spectrum could be observed for incubation times up to 12 h.

3.5. Comparison of relaxation times of different complexes

Finally, a comparison of relaxation properties of the whole series of macrocyclic complexes was performed in D_2O/glycerol-d_8. Corresponding transverse and longitudinal relaxation traces are shown in Fig. 6(a and b) and (c and d) in linear and semi-logarithmic representation. Differences in longitudinal relaxation within this series are basically negligible. This supports the assumption that the longitudinal relaxation of these complexes is predominantly due to the orbit lattice coupling and is thus very little affected by the strength of ZFS interaction or by the hyperfine interaction to surrounding magnetic nuclei.

The series of transverse relaxation measurements reveals more differences between different complexes. There is no apparent correlation between the strength of the ZFS interaction and the rate of Gd(III) transverse relaxation (Fig. 6(c and d)). In particular, the two stereoisomers of [Gd(M8DOTA)] have quite different ZFS (most probably, due to the different strength of the symmetry distortion) but, nevertheless, transverse relaxation is virtually the same in both cases (Fig. 7). The [Gd(M8DOTA)] and $[Gd(DOTAM)]^{3+}$

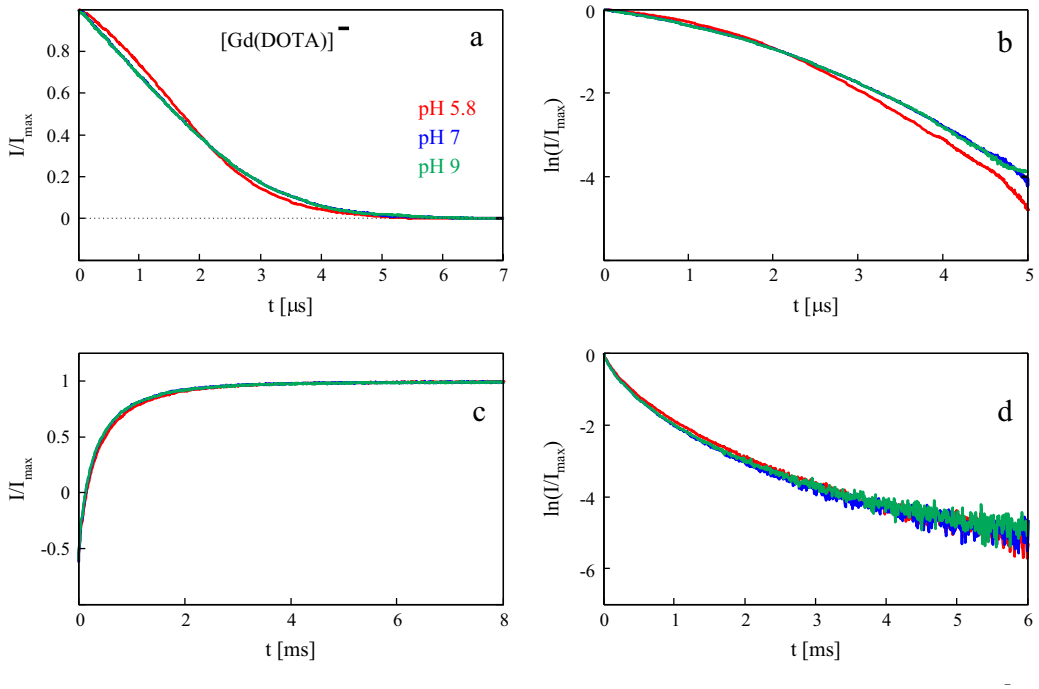

Fig. 5. pH dependency of the transverse (a and b) and longitudinal (c and d) relaxation times traces of $[Gd(DOTA)]^-$ in linear (a and c) and semilogarithmic (b and d) representation. Measurements were recorded at 10 K at Q band at different pH: red (pH 5.8), blue (pH 7) and green (pH 9). Buffer solution was prepared in H_2O and sample was diluted with glycerol. Each time trace was normalized to its maximum. (For interpretation of the references to color in this figure legend, the reader is referred to the web version of this article.)

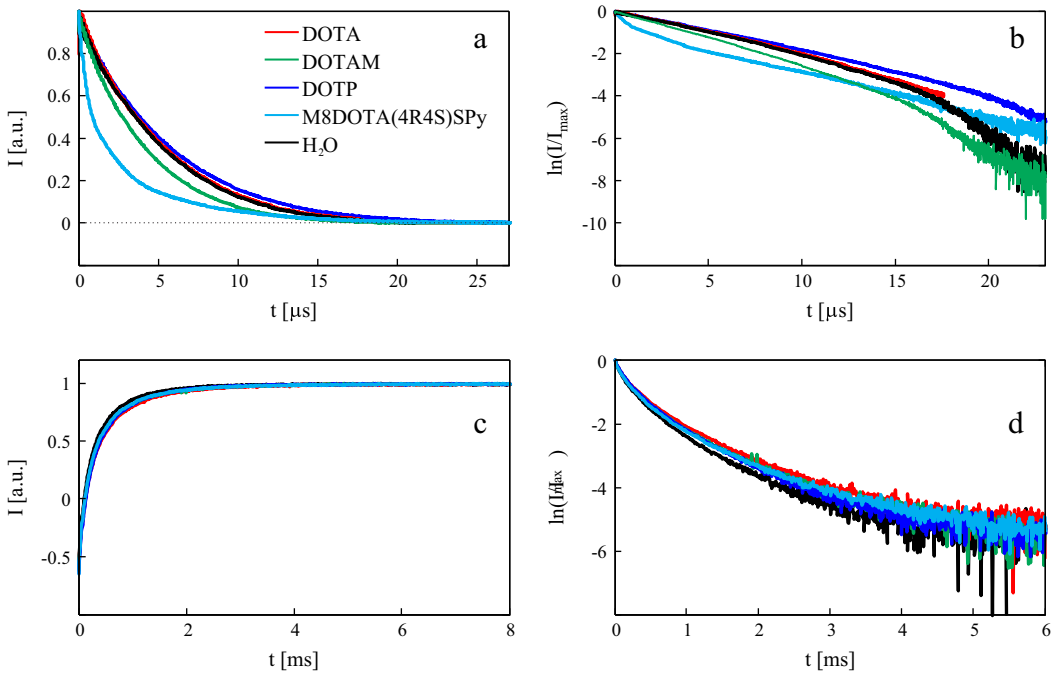

Fig. 6. Transverse (a and b) and longitudinal (c and d) relaxation times traces of Gd(III)-complexes in the linear (a and c) and semilogarithmic (b and d) representation. Measurements were recorded at 10 K at pH 5.8 and in a fully deuterated matrix (D_2O/glycerol-d_8) for: $[Gd(DOTA)]^-$ (red), $[Gd(DOTP)]^{5-}$ (blue), $[Gd(DOTAM)]^{3+}$ (green), [Gd(M8DOTA(4R4S)SPy)] (light blue), and $[Gd(III)]_{aq}$ (black). Each time trace was normalized to its maximum. (For interpretation of the references to color in this figure legend, the reader is referred to the web version of this article.)

complexes exhibit faster relaxation than other complexes, whereas the transverse relaxation of the water coordinated Gd(III) (abbreviated as $[Gd(III)]_{aq}$), $[Gd(DOTA)]^-$ and $[Gd(DOTP)]^{5-}$ is approximately the same with slight advantage for $[Gd(DOTP)]^{5-}$ at long times.

The particularly fast transverse relaxation of [Gd(M8DOTA)] should be, apparently, attributed to the presence of the eight methyl groups with 24 protons. At 10 K the rotational motion of these groups is frozen, but the proton tunneling is a known important source of relaxation [64]. Importantly, at long mixing times

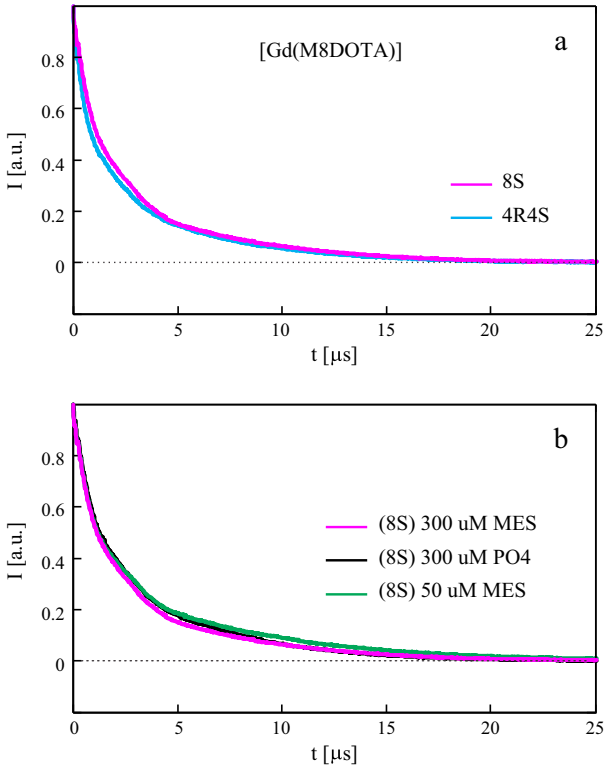

Fig. 7. Comparison of transverse relaxation properties for stereoisomers [Gd(M8DOTA(8S)SPy)] and [Gd(M8DOTA(4R4S)SPy)] (a), and comparison of the transverse relaxation properties of [Gd(M8DOTA(8S)SPy)] in MES and phosphate buffer at the concentrations of the chelate complexes of 50 μM and 300 μM (b). Magenta: 300 μM [Gd(M8DOTA(8S)SPy)] in MES buffer; black: 300 μM [Gd(M8DOTA(8S)SPy)] in phosphate buffer; green: 50 μM [Gd(M8DOTA(8S)SPy)] in MES buffer; light blue: 300 μM [Gd(M8DOTA(4R4S)SPy)] in MES buffer. Measurements were performed at 10 K. (For interpretation of the references to color in this figure legend, the reader is referred to the web version of this article.)

the transverse relaxation of [Gd(M8DOTA)] is not so much slower than for other complexes, and the maximum achievable length of the e.g. DEER trace would be only ~2 μs shorter. The complexes of M8DOTA with lanthanide ions are particularly favorable in paramagnetic NMR experiments [49]. Therefore, despite somewhat worse relaxation properties in pulse EPR, these complexes might appear particularly well performing for the combined NMR/EPR approaches.

One can further speculate that somewhat faster relaxation of the $[Gd(DOTAM)]^{3+}$ is connected to the presence of the extra four ^{14}N nuclei in addition to the nitrogen quartet in the tetraazacyclododecane ring. However, generalizing this to a statement that magnetic nuclei in the chelator molecule lead to faster transverse relaxation might not be possible, since, for instance, the presence of four phosphate groups in DOTP does not increase the relaxation, despite higher magnetic moment of ^{31}P as compared to the ^{14}N (in DOTAM). It might be thus possible that the change of transverse relaxation is not always directly induced by the magnetic nuclei within the chelator molecule, but might also be due to the solvent molecules arrangement around the particular chelate complex. Unlike DOTAM and DOTA, it is known that $[Gd(DOTP)]^{5-}$ forms a strong framework of hydrogen bonds in its second solvation sphere and that it lacks a H_2O directly bound to the metal center [65]. These two features might be beneficial in the design of chelators with particularly slow Gd(III) relaxation times.

The transverse relaxation traces of [Gd(M8DOTA)] possess two kinks and thus consist of at least three distinct components (Fig. 7). It is reasonable to attribute different relaxation components to the few possible conformations of [Gd(M8DOTA)] [49], possibly including the arrangement of solvation molecules. Furthermore, one water molecule would have a possibility of directly coordinating to Gd(III) in such a complex thus providing possibility of further components in the relaxation trace. The transverse relaxation of the [Gd(M8DOTA)] complexes is identical in MES buffer (200 mM) and phosphate buffer (20 mM), indicating rather small effect of ^{31}P nuclei distributed at millimolar concentration in the glassy matrix on the relaxation of Gd(III). Only a very small difference in transverse relaxation was observed for [Gd(M8DOTA(8S)SPy)] with concentrations of 50 μM and 300 μM (Fig. 7b), thus indicating almost no electron spin diffusion contribution.

4. Discussion and conclusions

The qualitative picture presented in this work demonstrates that despite being weak as compared to the ZFS interaction the hyperfine couplings to surrounding nuclei play an important, sometimes critical role for the spectroscopic properties of Gd(III) chelate complexes. This primarily concerns the central transition of Gd(III), which is most important for PDS measurements, and for which the contribution of ZFS to the line width is strongly reduced compared to other transitions. Fortunately for the biochemical applications of Gd(III)-based spin labels, our results demonstrate that Gd(III) relaxation properties are rather weakly changing with pH or buffer type, thus making the labels broadly applicable and reliable. The effect of solvent deuteration on transverse relaxation of Gd(III) is nearly as strong as it is for organic radicals [15,47]. Importantly, the main mechanism responsible for the transverse relaxation of the central transition of Gd(III) seems to switch between protonated and deuterated matrices, being mostly driven by nuclear spin diffusion in the former case. In the latter case it is difficult to discriminate any mechanism, based on the qualitative considerations we reported here. However, strong change of the transverse relaxation of [Gd(M8DOTA)] as compared to other complexes, as well as nearly no change for the two [Gd(M8DOTA)] stereoisomers with rather different ZFS suggest that hyperfine interaction with magnetic nuclei of the chelator molecule might play a significant role in the transverse relaxation of Gd(III) centers. Furthermore, the example of DOTP demonstrates that the directly coordinated as well as the second solvation sphere molecules can influence relaxation properties and ZFS of Gd(III) centers. The echo reduction in Gd(III)–nitroxide DEER measurements also demonstrates a clear dependence on hyperfine interactions with solvent molecules.

The relative rate of transverse relaxation for the central transition of Gd(III) is important whenever details of spin dynamics of such paramagnetic centers are considered. In such studies one has to take into account the different regimes shown in Fig. 4. Furthermore, as it is apparent from Fig. 6, the difference between transverse and longitudinal relaxation rates for Gd(III) chelate complexes in fully deuterated matrices can be less than two orders of magnitude. In such cases, e.g. in very long distance measurements with Gd(III)–Gd(III) DEER, the longitudinal relaxation might need to be considered for proper data analysis.

Regarding the optimization of PDS experiments, one conclusion of this work is that magnetic nuclei should be avoided whenever possible when designing the new chelating molecules. Our study, thus, suggests that the Gd(III) tags optimized for MRI that allow for one or more directly coordinated water molecules might be sub-optimal for the PDS measurements, and that tags that leave no possibility of directly coordinated solvent molecules might perform better in terms of transverse relaxation of Gd(III). Concerning the Gd(III)–nitroxide DEER experiments, our study confirms previous theoretical predictions that DEER echo reduction in such experiment is ZFS dependent. The increase of the DEER echo

reduction with decreasing the strength of ZFS interaction counteracts the sensitivity improvement due to narrowing of the central transition of Gd(III). Thus, in the Gd(III)–nitroxide DEER the use of Gd(III) complexes with smaller ZFS is expected to bring significantly less improvement in the signal-to-noise ratio, as compared to Gd(III)–Gd(III) DEER. However, sample deuteration appears to bring an additional advantage for this experiment as DEER echo reduction is measurably weaker for deuterated samples.

Overall, we believe that this work provides a useful overview of the spectroscopic properties of Gd(III) centers based on tetraazacyclododecane derivatives, with respect to their applications in PDS.

Acknowledgments

We wish to thank Dr. Roche Walliser (Uni Basel) for help in the synthesis of M8DOTA(4R4S)Spy. The Swiss National Science Foundation is acknowledged for a Grant No. SNF 200021_130263 (to D.H.) and a Grant No. SNF 200020_14441 (L.G., M.Y.). Prof. Dr. Gunnar Jeschke, the head of the EPR group at the Laboratory of Physical Chemistry at ETH Zurich, is acknowledged for the support of this project, numerous discussions, and critical reading of the manuscript.

Appendix A. Supplementary material

Supplementary data associated with this article can be found, in the online version, at http://dx.doi.org/10.1016/j.jmr.2015.08.009.

References

[1] A.D. Milov, K.M. Salikhov, M.D. Shirov, Use of the double resonance in electron spin echo method for the study of paramagnetic center spacial distribution in solids, Fiz. Tverd. Tela (Leningrad) 23 (1981) 975–982.
[2] A.D. Milov, A.B. Pomarev, Y.D. Tsvetkov, Electron electron double resonance in electron-spin echo-model biradical systems and the sensitized photolysis of decalin, Chem. Phys. Lett. 110 (1984) 67–72.
[3] R.E. Martin, M. Pannier, F. Diederich, V. Gramlich, M. Hubrich, H.W. Spiess, Determination of end-to-end distances in a series of TEMPO diradicals of up to 2.8 nm length with a new four-pulse double electron electron resonance experiment, Angew. Chem., Int. Ed. Engl. 37 (1998) 2834–2837.
[4] M. Pannier, S. Veit, A. Godt, G. Jeschke, H.W. Spiess, Dead-time free measurements of dipole–dipole interactions between electron spins, J. Magn. Reson. 142 (2000) 331–340.
[5] L.V. Kulik, S.A. Dzuba, I.A. Grigoryev, Y.D. Tsvetkov, Electron dipole–dipole interaction in ESEEM of nitroxide biradicals, Chem. Phys. Lett. 343 (2001) 315–324.
[6] S. Milikisyants, F. Scarpelli, M.G. Finiguerra, M. Ubbink, M.A. Huber, A pulsed EPR method to determine distances between paramagnetic centers with strong spectral anisotropy and radicals: the dead-time free RIDME sequence, J. Magn. Reson. 201 (2009) 48–56.
[7] S. Razzaghi, M. Qi, A.I. Nalepa, A. Godt, G. Jeschke, A. Savitsky, M. Yulikov, RIDME spectroscopy with Gd(III) centers, J. Phys. Chem. Lett. 5 (2014) 3970–3975.
[8] P.P. Borbat, J.H. Freed, Multiple-quantum ESR and distance measurements, Chem. Phys. Lett. 313 (1999) 145–154.
[9] G. Jeschke, M. Pannier, A. Godt, H.W. Spiess, Dipolar spectroscopy and spin alignment in electron paramagnetic resonance, Chem. Phys. Lett. 331 (2000) 243–252.
[10] C. Altenbach, T. Marti, H.G. Khorana, W.L. Hubbell, Transmembrane protein structure: spin labeling of bacteriorhodopsin mutants, Science 248 (1990) 1088–1092.
[11] J.P. Klare, H.-J. Steinhoff, Spin labeling EPR, Photosynth. Res. 102 (2009) 377–390.
[12] E. Bordignon, Site-directed spin labeling of membrane proteins, Curr. Top. Chem. 321 (2012) 121–157.
[13] W.L. Hubbell, D.S. Cafiso, C. Altenbach, Identifying conformational changes with site-directed spin labeling, Nat. Struct. Biol. 7 (2000) 735–739.
[14] G. Jeschke, Y. Polyhach, Distance measurements on spin-labelled biomacromolecules by pulsed electron paramagnetic resonance, Phys. Chem. Chem. Phys. 9 (2007) 1895–1910.
[15] R. Ward, A. Bowman, E. Sozudogru, H. El-Mkami, T. Owen-Hughes, D.G. Norman, EPR distance measurements in deuterated proteins, J. Magn. Reson. 207 (2010) 164–167.
[16] O. Schiemann, T.F. Prisner, Long-range distance determination in biomacromolecules by EPR spectroscopy, Q. Rev. Biophys. 40 (2007) 1–53.
[17] G. Jeschke, DEER distance measurements on proteins, Ann. Rev. Phys. Chem. 63 (2012) 1–28.
[18] O. Duss, E. Michel, M. Yulikov, M. Schubert, G. Jeschke, F.H.-T. Allain, Structural basis of the non-coding RNA RsmZ acting as a protein sponge, Nature 509 (2014) 588–592.
[19] R. Ward, M. Zoltner, L. Beer, H. El Mkami, I.R. Henderson, T. Palmer, D.G. Norman, The orientation of a tandem POTRA domain pair, of the beta-barrel assembly protein BamA, determined by PELDOR spectroscopy, Structure 17 (2009) 1187–1194.
[20] I. Smirnova, V. Kasho, J.-Y. Choe, C. Altenbach, W.L. Hubbell, H.R. Kaback, Sugar binding induces an outward facing conformation of LacY, Proc. Natl. Acad. Sci. USA 104 (2007) 16504–16509.
[21] X. Han, J.H. Bushweller, D.S. Cafiso, L.K. Tamm, Membrane structure and fusion-triggering conformational change of the fusion domain from influenza hemagglutinin, Nat. Struct. Biol. 8 (2001) 715–720.
[22] S. Bleicken, G. Jeschke, C. Stegmueller, R. Salvador-Gallego, A.J. García-Sáez, E. Bordignon, Structural model of active Bax at the membrane, Mol. Cell 56 (2014) 496–505.
[23] I. Hanelt, D. Wunnicke, E. Bordignon, H.J. Steinhoff, D.J. Slotboom, Conformational heterogeneity of the aspartate transporter Glt(Ph), Nat. Struct. Biol. 20 (2013) 210–214.
[24] E.R. Georgieva, P. Borbat, C. Ginter, J.H. Freed, O. Boudker, Conformational ensemble of the sodium-coupled aspartate transporter, Nat. Struct. Biol. 20 (2013) 215–221.
[25] A.M. Raitsimring, C. Gunanathan, A. Potapov, I. Efremenko, J.M.L. Martin, D. Milstein, D. Goldfarb, Gd^{3+} complexes as potential spin labels for high field pulsed EPR distance measurements, J. Am. Chem. Soc. 129 (2007) 14138–14139.
[26] I. Kaminker, I. Tkach, N. Manukovsky, T. Huber, H. Yagi, G. Otting, M. Bennati, D. Goldfarb, W-band orientation selective DEER measurements on a Gd^{3+}/nitroxide mixed-labeled protein dimer with a dual mode cavity, J. Magn. Reson. 227 (2013) 66–71.
[27] P. Lueders, G. Jeschke, M. Yulikov, Double electron–electron resonance measured between Gd^{3+} ions and nitroxide radicals, J. Phys. Chem. Lett. 2 (2011) 604–609.
[28] M. Yulikov, P. Lueders, M.F. Warsi, V. Chechik, J. Jeschke, Distance measurements in Au nanoparticles functionalized with nitroxide radicals and Gd^{3+}–DTPA chelate complexes, Phys. Chem. Chem. Phys. 14 (2012) 10732–10746.
[29] L. Garbuio, E. Bordignon, E.K. Brooks, W.L. Hubbell, G. Jeschke, M. Yulikov, Orthogonal spin labeling and Gd(III)–nitroxide distance measurements on bacteriophage T4-lysozyme, J. Phys. Chem. B 117 (2013) 3145–3153.
[30] A. Martorana, G. Bellapadrona, A. Feintuch, E. Di Gregorio, S. Aime, D. Goldfarb, Probing protein conformation in cells by EPR distance measurements using Gd^{3+} spin labeling, J. Am. Chem. Soc. 136 (2014) 13458–13465.
[31] C.D. Barry, J.A. Glasel, R.J.P. Williams, A.V. Xavier, Quantitative determination of conformations of flexible molecules in solution using lanthanide ions as nuclear magnetic resonance probes: application to adenosine-5′-monophosphate, J. Mol. Biol. 84 (1974) 471–490.
[32] P. Caravan, J.J. Ellison, T.J. McMurry, R.B. Lauffer, Gadolinium(III) chelates as MRI contrast agents: structure, dynamics, and applications, Chem. Rev. 99 (1999) 2293–2352.
[33] E. Boros, E.M. Gale, P. Caravan, MR imaging probes: design and applications, Dalton Trans. 44 (2015) 4804–4818.
[34] A.M. Raitsimring, A.V. Astashkin, P. Caravan, High-frequency EPR and ENDOR characterization of MRI contrast agent. Biological magnetic resonance, in: L. Berliner, G. Hanson (Eds.), High Resolution EPR: Applications to Metalloenzymes and Metals in Medicine, vol. 28, Springer, New York, 2009, pp. 581–621.
[35] A.M. Raitsimring, A.V. Astashkin, O.G. Poluektov, P. Caravan, High-field pulsed EPR and ENDOR of Gd^{3+} complexes in glassy solutions, Appl. Magn. Reson. 28 (2005) 281–295.
[36] M. Benmelouka, J. Van Tol, A. Borel, M. Port, L. Helm, L.C. Brunel, A.E. Merbach, A high-frequency EPR study of frozen solutions of Gd-III complexes: straightforward determination of the zero-field splitting parameters and simulation of the NMRD profiles, J. Am. Chem. Soc. 128 (2006) 7807–7816.
[37] A. Hudson, J.W.E. Lewis, Electron spin relaxation of S-8 ions in solution, Trans. Faraday Soc. 66 (1971) 1297–1301.
[38] S. Rast, P.H. Fries, E. Belorizky, Static zero field splitting effects on the electronic relaxation of paramagnetic metal ion complexes in solution, J. Chem. Phys. 113 (2000) 8724–8735.
[39] M. Benmelouka, A. Borel, L. Moriggi, L. Helm, A.E. Merbach, Design of Gd(III)-based magnetic resonance imaging contrast agents: Static and transient zero-field splitting contributions to the electronic relaxation and their impact on relaxivity, J. Phys. Chem. B 111 (2007) 832–840.
[40] A. Borel, J.F. Bean, R.B. Clarkson, L. Helm, L. Moriggi, A.D. Sherry, M. Woods, Towards the rational design of MRI contrast agents: electron spin relaxation is largely unaffected by the coordination geometry of Gadolinium(III)–DOTA-type complexes, Chem. Eur. J. 14 (2008) 2658–2667.
[41] A.V. Astashkin, A.M. Raitsimring, Electron spin echo envelope modulation theory for high electron spin systems in weak crystal field, J. Chem. Phys. 117 (2002) 6121–6132.
[42] P. Lueders, H. Jager, M.A. Hemminga, G. Jeschke, M. Yulikov, Distance measurements on orthogonally spin-labeled membrane spanning WALP23 polypeptides, J. Phys. Chem. B 117 (2013) 2061–2068.
[43] F. Bloch, A. Siegert, Magnetic resonance for nonrotating fields, Phys. Rev. 57 (1940) 522–527.

[44] M.K. Bowman, A.G. Maryasov, Dynamic phase shifts in nanoscale distance measurements by double electron electron resonance (DEER), J. Magn. Reson. 185 (2007) 270–282.
[45] I. Kaminker, H. Yagi, T. Huber, A. Feintuch, G. Otting, D. Goldfarb, Spectroscopic selection of distance measurements in a protein dimer with mixed nitroxide and Gd^{3+} spin labels, Phys. Chem. Chem. Phys. 14 (2012) 4355–4358.
[46] A. Raitsimring, A. Dalaloyan, A. Collauto, A. Feintuch, T. Meade, D. Goldfarb, Zero field splitting fluctuations induced phase relaxation of Gd^{3+} in frozen solutions at cryogenic temperatures, J. Magn. Reson. 248 (2014) 71–80.
[47] M. Huber, M. Lindgren, P. Hammarstrom, L.-G. Martensson, U. Carlsson, G.R. Eaton, S.S. Eaton, Phase memory relaxation times of spin labels in human carbonic anhydrase II: Pulsed EPR to determine spin label location, Biophys. Chem. 94 (2001) 245–256.
[48] D. Goldfarb, Gd^{3+} spin labeling for distance measurements by pulse EPR spectroscopy, Phys. Chem. Chem. Phys. 16 (2014) 9685–9699.
[49] D. Häussinger, J. Huang, S. Grzesiek, DOTA-M8: an extremely rigid, high-affinity lanthanide chelating tag for PCS NMR spectroscopy, J. Am. Chem. Soc. 131 (2009) 14761–14767.
[50] Y. Song, T.J. Meade, A.V. Astashkin, E.L. Klein, J.H. Enemark, A. Raitsimring, Pulsed dipolar spectroscopy distance measurements in biomacromolecules labeled with Gd(III) markers, J. Magn. Reson. 210 (2011) 59–68.
[51] B. Joseph, V.M. Korkhov, M. Yulikov, G. Jeschke, E. Bordignon, Conformational cycle of the vitamin B-12 ABC Importer in liposomes detected by double electron–electron resonance (DEER), J. Biol. Chem. 289 (2014) 3176–3185.
[52] A. Barge, G. Cravotto, E. Gianolio, F. Fedeli, How to determine free Gd and free ligand in solution of Gd chelates. A technical note, Contrast Media Mol. Imaging 8 (2006) 184–188.
[53] I. Gromov, J. Shane, R. Forrer, R. Rakhmatoullin, Y. Rozentzwaig, A. Schweiger, A Q-band pulse EPR/ENDOR spectrometer and the implementation of advanced one- and two-dimensional pulse EPR methodology, J. Magn. Reson. 149 (2001) 196–203.
[54] R. Tschaggelar, B. Kasumaj, M.G. Santangelo, J. Forrer, H. Leger, F. Dube, F. Diederich, J. Harmer, I. Schumann, I. Garcia-Rubio, G. Jeschke, Cryogenic 35 GHz pulse ENDOR probehead accommodating large sample sizes: performances and applications, J. Magn. Reson. 200 (2009) 81–87.
[55] S. Stoll, A. Schweiger, EasySpin, a comprehensive software package for spectral simulation and analysis in EPR, J. Magn. Reson. 178 (2006) 42–55.
[56] A. Volkov, C. Dockter, T. Bund, H. Paulsen, G. Jeschke, Pulsed EPR determination of water accessibility to spin-labeled amino acid residues in LHCIIb, Biophys. J. 96 (2009) 1124–1141.
[57] D. Leporini, V. Schadler, U. Wiesner, H.W. Spiess, G. Jeschke, Electron spin relaxation due to small-angle motion: theory for the canonical orientations and application to hierarchic cage dynamics in ionomers, J. Chem. Phys. 119 (2003) 11829–11846.
[58] P. Schoeps, P.E. Spindler, A. Marko, T.F. Prisner, Broadband spin echoes and broadband SIFTER in EPR, J. Magn. Reson. 250 (2015) 55–62.
[59] A. Doll, S. Pribitzer, R. Tschaggelar, G. Jeschke, Adiabatic and fast passage ultra-wideband inversion in pulsed EPR, J. Magn. Reson. 230 (2013) 27–39.
[60] P.E. Spindler, S.J. Glaser, T.E. Skinner, T.F. Prisner, Broadband inversion PELDOR spectroscopy with partially adiabatic shaped pulses, Angew. Chem., Int. Ed. 52 (2013) 3425–3429.
[61] A. Doll, G. Jeschke, Fourier-transform electron spin resonance with bandwidth-compensated chirp pulses, J. Magn. Reson. 246 (2014) 18–26.
[62] A. Bianchi, L. Calabi, F. Corana, S. Fontana, P. Losi, A. Maiocchi, L. Paleari, B. Valtancoli, Thermodynamic and structural properties of Gd(III) complexes with polyamino-polycarboxylic ligands: basic compounds for the development of MRI contrast agents, Coord. Chem. Rev. 204 (2000) 309–393.
[63] A.D. Sherry, P. Caravan, R.E. Lenkinski, Primer on gadolinium chemistry, J. Magn. Reson. Imaging 30 (2009) 1240–1248.
[64] A. Zecevic, G.R. Eaton, S.S. Eaton, M. Lindgren, Dephasing of electron spin echoes for nitroxyl radicals in glassy solvents by non-methyl and methyl protons, Mol. Phys. 95 (1998) 1255–1263.
[65] S. Aime, M. Botta, D. Parker, J.A.G. Williams, Extent of hydration of octadentate lanthanide complexes incorporating phosphinate donors: solution relaxometry and luminescence studies, J. Chem. Soc., Dalton Trans. (1996) 17–23.